Evaluation and design of a large-scale cloaking device by the Hamiltonian-based ray-tracing method. Part II: design of the distribution of constitutive parameters

Tanaka, Tatsuo

Matoba, Osamu

(Citation)
Journal of the Optical Society of America B,34(5):1052-1059

(Issue Date)
2017-05-01

(Resource Type)
journal article

(Version)
Accepted Manuscript

Evaluation and design of a large-scale cloaking device by Hamiltonian-based ray-tracing method. Part II: Design of the Distribution of Constitutive Parameters

Tatsuo Tanaka,[1,2,*] Osamu Matoba[1]

[1]*Deparrtment of Systems Science, Graduate School of System Informatics, Kobe University, Rokkodai 1-1, Nada, Kobe 657-8501, Japan*
[2]*Computer Aided Engineering Dept., Production Technology Center, Corporate Production Technology, Asahi Kasei Corporation, 1-3-2, Yakoh, Kawasaki, Kawasaki, Kanagawa 210-0863, Japan*
**Corresponding author: tanaka.tdn@om.asahi-kasei.co.jp*

Received XX Month XXXX; revised XX Month, XXXX; accepted XX Month XXXX; posted XX Month XXXX (Doc. ID XXXXX); published XX Month XXXX

Improvement in cloaking performance by the design of distributions of the constitutive parameters is investigated. The distributions are changed by employing the Navier's equation with various distributions of Young's modulus as the partial differential equation for the solution of the Jacobian transformation matrix used in transformation optics. The cloaking performance is evaluated by Hamiltonian-based ray tracing. The numerical results show the proposed design method can improve the cloaking performance. The design method can contribute to realizing large-scale cloaking devices by taking account of the finite resolution of the manufacture.

OCIS codes: *(080.2710) Inhomogeneous optical media; (080.2740) Geometric optical design; (080.5692) Ray trajectories in inhomogeneous media; (160.3918) Metamaterials; (220.2740) Geometric optical design; (230.3205) Invisibility cloaks.*

http://dx.doi.org/10.1364/AO.99.099999

1. Introduction

Cloaking phenomena [1-4] are considered to be potential for industrial applications such as transparent pillars of automobile bodies [5-7], transparent surgery-supporting robots [8] and highly efficient solar cells [9], thanks to the theoretical works of transformation optics [1, 2]. The pillar application is expected to reduce a dead zone in the view field of a driver, which can lead to the decline of the number of car accidents, and the transparent surgery-supporting robots can improve the usability of the operator. In addition, based on force-loaded transformation optics, force-induced transformational devices, such as an optical escalator, have been proposed [10].

For industrial applications, there are many issues to be solved. One of the issues is to design cloaking devices of a large size. For this purpose, the design and evaluation of cloaking devices are required. It has recently been possible to evaluate the performance of cloaking devices at optical frequencies by using Hamiltonian-based ray tracing [11–25]. The Hamiltonian-based ray tracing has been extended to arbitrary coordinate systems and curved spaces [26]. Besides cloaking devices, an Eaton lens [26] and a graded negative-index metamaterial magnifier [27] have been investigated by this method. Recently, a method called "force tracing" to trace the optical force has been proposed based on the Hamiltonian-based ray tracing [28].

In order to deal with cloaking devices with arbitrary shapes by the Hamiltonian-based ray tracing, two technical issues have to be solved. The first issue is how to represent the surface of a cloaking device. In Ref. 29, in order to represent the surface, the Hamiltonian-based ray-tracing method adapting a surface-mesh representation, where the surfaces of arbitrary shapes are modeled by mesh structure, has been proposed.

The other issue is how to design the constitutive parameters of cloaking devices with arbitrary shapes. This issue can be solved by the numerical method for the calculation of the constitutive parameters based on the finite element method (FEM) proposed in Ref. 30. In our previous work [31], we have proposed the Hamiltonian ray tracing adapting a full-mesh representation, where both the surface and the inside of a cloaking device are modeled by mesh structure in order to implement the numerical method for the calculation of the constitutive parameters.

From the analysis of cloaking devices by using our Hamiltonian ray tracing, the following problem for the design of cloaking devices has been revealed. A coarse full-mesh resolution causes the deterioration of cloaking performance, especially for the ray passing near the inner boundary. This deterioration is considered to be due to the abrupt changes of the relative permittivity and permeability near the inner boundary, which cannot be modelled at the coarse full-mesh resolution accurately. This problem will become very serious when cloaking devices are manufactured because current processing technologies can realize the distributions of constituent parameters not rigorously but with the finite resolution. The resolution depends on the processing method. If a processing method with a coarse resolution

can only be utilized for the manufacture of a cloaking device, the cloaking device will yield the deterioration of the cloaking performance. Therefore, the further designing method is required to improve the performance of cloaking devices fabricated at a coarse full-mesh resolution.

On the other hand, the distributions of the constituent parameters can be varied by changing the partial differential equation used in the numerical method for the calculation of the constitutive parameters based on the FEM [15].

In this paper, we propose a method to improve the performance of cloaking devices by designing the distributions of constitutive parameters. The distributions of the constituent parameters are varied by employing the Navier's equation with various distributions of Young's modulus as the partial differential equation used in the numerical method for the calculation of the constitutive parameters based on the FEM. The performance of a cylindrical cloaking device whose constitutive parameters were designed by this method is evaluated by the Hamiltonian ray tracing.

The rest of the paper is organized as follows. In CHAPTER 2, we describe the numerical method of the constitutive parameters of cloaking devices. In CHAPTER 3, we present the distributions of $\boldsymbol{\varepsilon}$ and $\boldsymbol{\mu}$ for various distributions of Young's modulus and the performance of the cylindrical cloaking device. In CHAPTER 4, we discuss the effects of Young's modulus on the distributions of $\boldsymbol{\varepsilon}$ and $\boldsymbol{\mu}$ and on the performance. Furthermore, we give a guideline for the numerical design of the constitutive parameters with the numerical result of a cloaking device with a totally arbitrary shape.

2. Calculation of Relative Permittivity Tensor and Permeability Tensor by Employing the Navier's Equation Method

The Hamiltonian-based ray tracing method and the evaluation method of the performance of cloaking devices are described in Ref. 31. Here, we present a proposed designing method of the relative permittivity and permeability by employing the Navier's equation to improve the cloaking performance. As described in Ref. 30, the relative permittivity tensor $\boldsymbol{\varepsilon}$ and relative permeability tensor $\boldsymbol{\mu}$ for cloaking devices with arbitrary shapes can be calculated by using the numerical method with the FEM-based solution of the Laplace's equation.

Besides the Laplace's equation, other partial differential equations can be employed to calculate the displacement field and the deformation gradient tensor [15], resulting in the different distributions of $\boldsymbol{\varepsilon}$ and $\boldsymbol{\mu}$. In this work, the Navier's equation, corresponding to the linear theory of elastic deformation of solids, is used to change the distributions of $\boldsymbol{\varepsilon}$ and $\boldsymbol{\mu}$. The Navier's equation is expressed as

$$-\nabla\cdot\boldsymbol{\tau}=0, \tag{1}$$

where $\boldsymbol{\tau}$ is the stress tensor given by

$$\boldsymbol{\tau}=\frac{Y}{2(1+\kappa)}\zeta+\frac{Y\kappa}{(1+\kappa)(1-2\kappa)}\mathrm{tr}(\zeta)\cdot\mathbf{I}, \tag{2}$$

where Y is the Young's modulus, κ the Poisson's ratio, $\mathbf{I}$ the identify matrix, tr(•) the trace function, and $\boldsymbol{\zeta}$ the strain tensor given by

$$\zeta=\frac{1}{2}\left(\nabla\boldsymbol{U}+(\nabla\boldsymbol{U})^{T}\right), \tag{3}$$

where $\boldsymbol{U}$ is the displacement field.

From Eqs. (1)-(3), the displacement field and the deformation gradient tensor can be changed by adjusting the distribution of Young's modulus, leading to various distributions of $\boldsymbol{\varepsilon}$ and $\boldsymbol{\mu}$. The solutions of the Laplace's equation and the Navier's equation are achieved based on the Finite Element Method (FEM) by employing the open source software, Elmer from CSC [32].

Since the FEM-based solution for $\boldsymbol{\varepsilon}$ and $\boldsymbol{\mu}$ are discretized in triangular mesh structure inside of a cloaking device, interpolation of $\boldsymbol{\varepsilon}$ and $\boldsymbol{\mu}$ is necessary for the Hamiltonian-based ray tracing. In this paper, $\boldsymbol{\varepsilon}$ and $\boldsymbol{\mu}$ are expressed as the linear functions of the components of a position vector inside each element used for the FEM-based solution of the Laplace's equation or the Navier's equation.

3. Numerical Results

3.1. Distributions of ε and μ for Various Distributions of Young's Modulus

The distributions of $\boldsymbol{\varepsilon}$ and $\boldsymbol{\mu}$ for the cylindrical cloaking device with the inner radius of 10mm and the outer radius of 30mm are obtained by the numerical method based on the FEM by employing the Navier's equation with various distributions of Young's modulus. We employ five full-mesh resolutions of 2.5, 1.0, 0.5, 0.25, and 0.10 mm. Here, a relative mesh resolution is defined as the ratio of a mesh size and a representative length of the cloaking device so that it can be universally applied to any other structure. As the representative length, the size of the cloaking device is adapted. The size corresponds to 60mm, the diameter of the inner cylinder of the cylindrical cloaking device. Therefore the relative mesh resolutions for 2.5, 1.0, 0.5, 0.25, and 0.10 mm correspond to 4.17e-02, 1.67e-02, 8.33e-03, 4.17e-03, and 1.67e-03. Hereafter, we investigate the numerical results based on the relative mesh resolution.

The value of the Young's modulus (Y) depends on the distance between the position and the center of the cylinder represented by d. In this study, the following seven distributions are considered: (i) $Y=d^{-5}$, (ii) $Y=d^{-3}$, (iii) $Y=d^{-1}$, (vi) $Y=d^{0}$, (v) $Y=d^{1}$, (vi) $Y=d^{3}$, and (vii) $Y=d^{5}$. Shown in Fig. 1 are the seven distributions of Young's modulus. As a reference, the distributions of $\boldsymbol{\varepsilon}$ and $\boldsymbol{\mu}$ for the cylindrical cloaking device are also calculated for the Laplace's equation. Here, since we assume that the cloaking media are impedance-matched with the surrounding medium, $\boldsymbol{\varepsilon}$ is equal to $\boldsymbol{\mu}$. Hence, we show only the calculation result of $\boldsymbol{\varepsilon}$ hereafter.

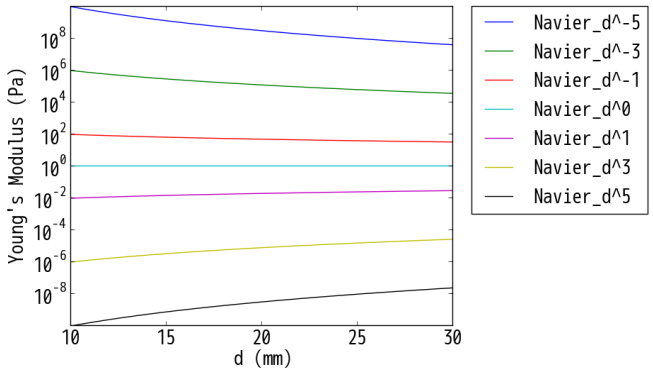

Fig. 1. The various distributions of Young's modulus.

The calculated distributions of the three principal permittivity, ε_r, ε_ϕ, and ε_z for the Laplace's equation at the relative full-mesh resolution of 1.67e-03 are depicted in Fig. 2. The principal axes for ε_r, ε_ϕ and ε_z are the radial axis, the azimuthal axis, and the z axis. From Fig. 2, each distribution is found to have the axial symmetry. This is the case for the Navier's equation with various distributions of Y.

Shown in Fig. 3 are the profiles of ε_r, ε_ϕ and ε_z along the radial axis at the relative full-mesh resolution of 1.67e-03. In addition, the profiles of

ε_ϕ near the inner boundary and the outer boundary are extended in Fig. 4. We can notice common features for the different distributions of Y in each of the three principle permittivity as follows. ε_ϕ is found to increase drastically near the inner boundary, while ε_r and ε_z approach 0.0, which means superluminal propagation. These features are required to realize invisibility cloaking.

In general, the three principle permittivity of the cylindrical cloaking device with the inner radius of a and the outer radius of b can be expressed by considering the space transformation from (r, ϕ, z) to (r', ϕ', z') as [1]

$$\varepsilon_r = \frac{f \cdot r}{r'}, \quad \textbf{(4a)}$$

$$\varepsilon_\phi = \frac{r}{f \cdot r'}, \quad \textbf{(4b)}$$

$$\varepsilon_z = \frac{r}{f \cdot r'}, \quad \textbf{(4c)}$$

where f *is* the derivative of r' with respect of r expressed as

$$f = \frac{dr'}{dr}, \quad \textbf{(5)}$$

Equations (4a)-(4c) can explain the features described above as follows,

$$r' \to a,\ r \to 0 \Rightarrow\ \varepsilon_r \to 0,\ \varepsilon_\phi \to \infty,\ \varepsilon_z \to 0, \quad \textbf{(6)}$$

In contrast, the variation of distribution of Y can result in the following differences in the profiles. The increase rate of ε_r and the decrease rate of ε_ϕ with the increase of d can be changed. The increase rate of ε_r becomes larger with changing from $Y=d^{-5}$ to $Y=d^5$, leading to the increase of the value of ε_r at the outer boundary in the same order. On the other hand, the decrease rate of ε_ϕ decreases in the same order, resulting in the decrease of the value of ε_ϕ at the outer boundary in the same order. We can notice that the profiles of ε_z have a turning point around d=22mm. The increase rate of ε_z increase with changing from $Y=d^{-5}$ to $Y=d^5$ in the range between the inner boundary and the turning point, while it increases with changing from $Y=d^5$ to $Y=d^{-5}$ in the range between the turning point and the outer boundary. This leads to the increase of the value of ε_z at the outer boundary with changing from $Y=d^5$ to $Y=d^{-5}$.

By comparing the profiles from the Navier's equation and the Laplace's equation, it is found that the profiles from Laplace's equation is very similar to those from the Navier's equation with $Y=d^0$.

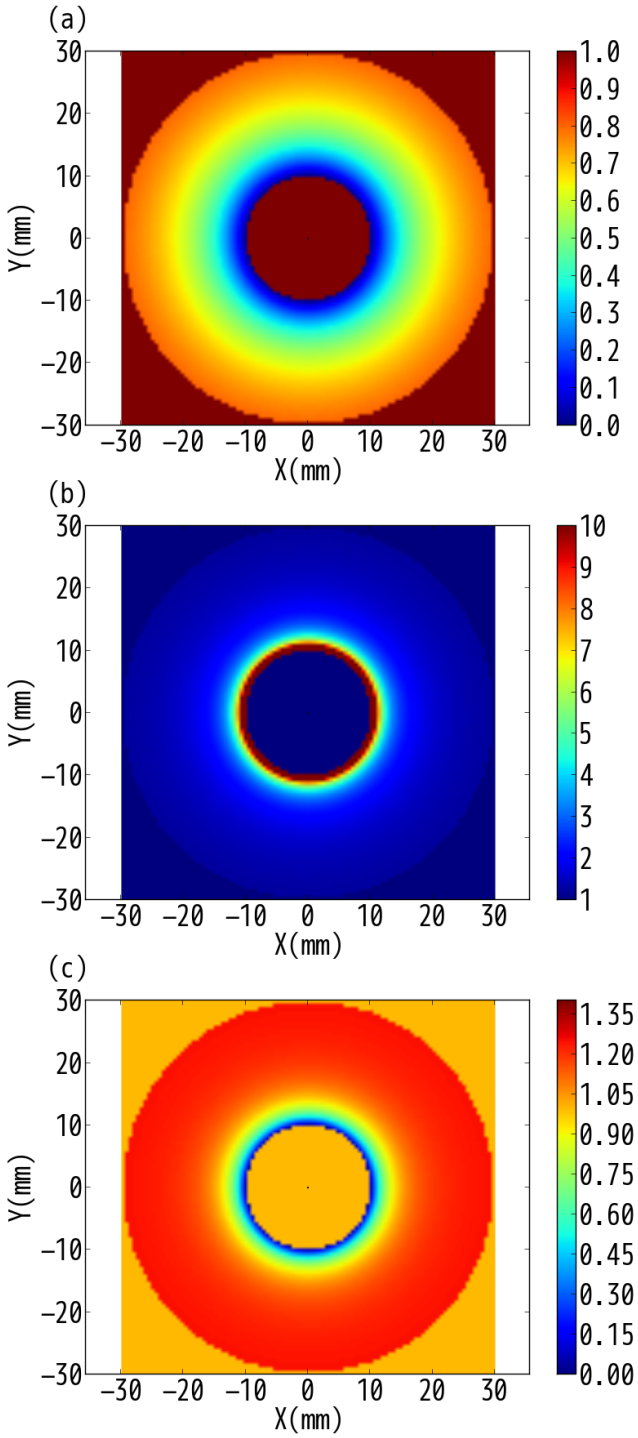

Fig. 2. The distributions of the three principle permittivity, (a) ε_r, (b) ε_ϕ, and (c) ε_z for the Laplace's equation.

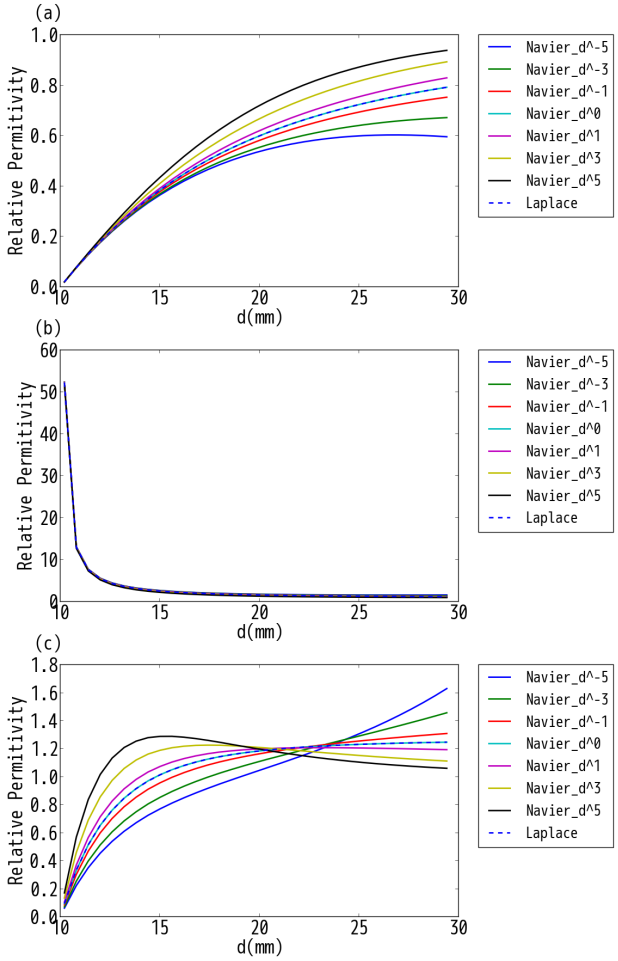

Fig. 3. The profiles of (a) ε_r, (b) ε_ϕ and (c) ε_Z along the radial axis.

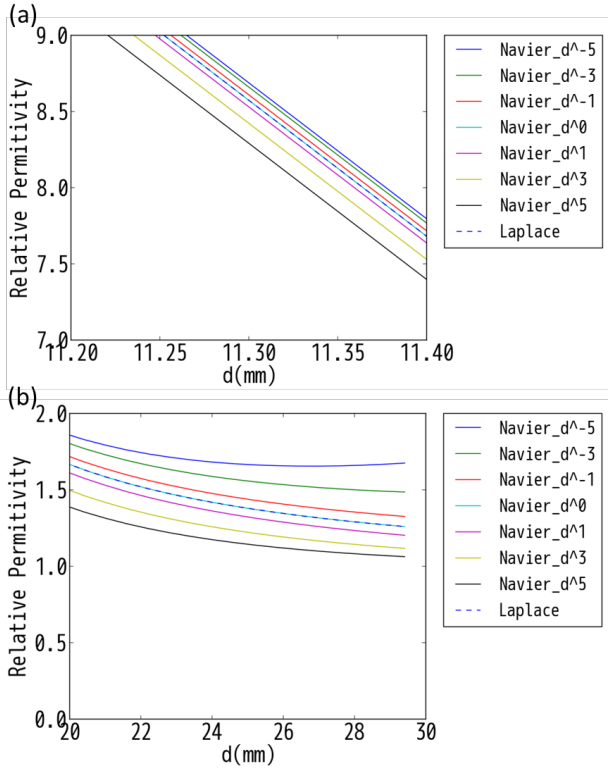

Fig. 4. The profiles of ε_ϕ along the radial axis; (a) near the inner boundary, (b) near the outer boundary.

3.2. Performances for Various Young's modulus

We calculate the performance of the cylindrical cloaking device by the Hamiltonian-based ray tracing with the distributions of $\boldsymbol{\varepsilon}$ and $\boldsymbol{\mu}$ obtained in 3.1. The cloaking device is represented by the full-mesh representation with five relative full-mesh resolutions of 4.17e-02, 1.67e-02, 8.33e-03, 4.17e-03, and 1.67e-03, which are employed for the calculation of the distributions of $\boldsymbol{\varepsilon}$ and $\boldsymbol{\mu}$.

Table 1 summarizes the calculated cloaking performance. From Table 1, we can notice the tendency that the cloaking performance becomes better with changing from $Y=d^5$ to $Y=d^{-5}$. Especially, at the relative full-mesh resolution of 4.17e-03, this trend is found to be distinct.

The ray trajectories obtained for the relative full-mesh resolutions of 4.17e-03 are illustrated in Fig. 5. The dependence of the cloaking performance on the radiation angle for the relative full-mesh resolutions of 4.17e-03 is shown in Fig. 6. From Figs. 5 and 6, the performance is found to be deteriorated around the radiation angle of 0.0 for the Navier's equation with $Y=R^m$ (m=-1, 1, 3, and 5) as well as for the Laplace's equation. On the other hand, it is found to be improved for $Y=R^m$ (m=-3, -5) in comparison with the Laplace's equation, which suggests the possibility that the variation of the distribution of Y can improve the cloaking performance.

In addition, the performance for the Laplace's equation is found to be similar to that for the Navier's equation with $Y=d^0$. This is because the two cases have very similar distributions of $\boldsymbol{\varepsilon}$ and $\boldsymbol{\mu}$ as described in 3.1.

Table 1: Performances of cylindrical cloaking calculated for the distributions of ε and μ obtained by the FEM-based solution of the Navier's equation with various distribution of Young's modulus (*Y*) and the Laplace's equation.

Number	Relative full-mesh resolution	Equations		Δθ(°)
1	4.17e-02	Navier's Eq.	$Y=d^{-5}$	11.1
2			$Y=d^{-3}$	11.7
3			$Y=d^{-1}$	12.2
4			$Y=d^{0}$	12.4
5			$Y=d^{1}$	12.9
6			$Y=d^{3}$	13.1
7			$Y=d^{5}$	14.2
8		Laplace's Eq.		12.1
9	1.67e-02	Navier's Eq.	$Y=d^{-5}$	4.12
10			$Y=d^{-3}$	5.04
11			$Y=d^{-1}$	5.31
12			$Y=d^{0}$	5.26
13			$Y=d^{1}$	5.32
14			$Y=d^{3}$	6.74
15			$Y=d^{5}$	7.20
16		Laplace's Eq.		5.19
17	8.33e-03	Navier's Eq.	$Y=d^{-5}$	4.26
18			$Y=d^{-3}$	4.12
19			$Y=d^{-1}$	4.50
20			$Y=d^{0}$	4.63
21			$Y=d^{1}$	4.62
22			$Y=d^{3}$	4.70
23			$Y=d^{5}$	4.61
24		Laplace's Eq.		4.51
25	4.17e-03	Navier's Eq.	$Y=d^{-5}$	0.729
26			$Y=d^{-3}$	0.887
27			$Y=d^{-1}$	1.46
28			$Y=d^{0}$	1.51
29			$Y=d^{1}$	2.48
30			$Y=d^{3}$	2.74
31			$Y=d^{5}$	1.74
32		Laplace's Eq.		1.43
33	1.67e-03	Navier's Eq.	$Y=d^{-5}$	0.144
34			$Y=d^{-3}$	0.198
35			$Y=d^{-1}$	0.108
36			$Y=d^{0}$	0.154
37			$Y=d^{1}$	0.151
38			$Y=d^{3}$	0.340
39			$Y=d^{5}$	0.374
40		Laplace's Eq.		0.113

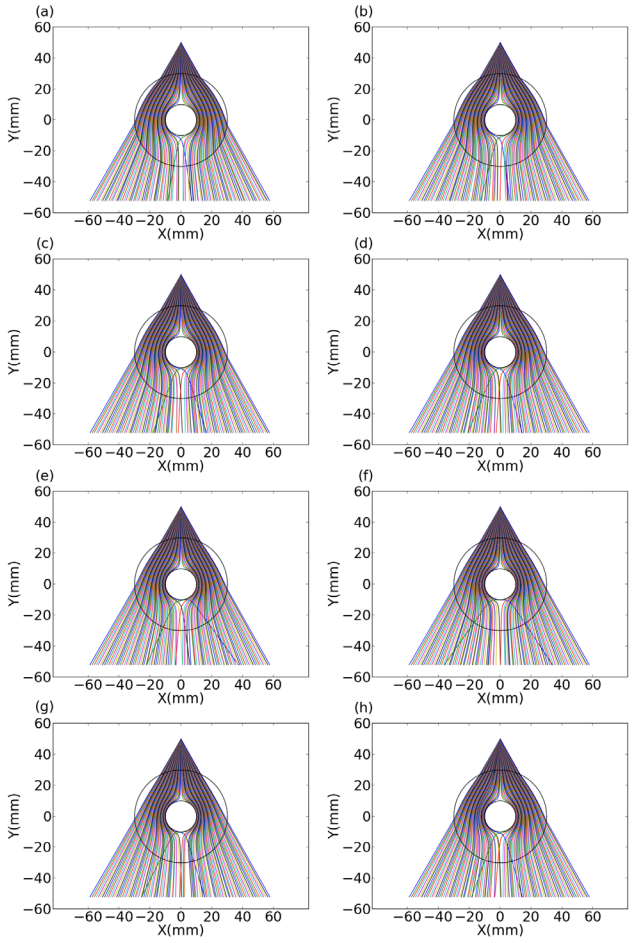

Fig. 5. The ray paths with the cylindrical cloaking device for the distributions of **ε** and **μ** obtained by the FEM-based solution of the Navier's equation with various distribution of Young's modulus (*Y*); (a) $Y = d^{-5}$, (b) $Y = d^{-3}$, (c) $Y = d^{-1}$, (d) $Y = d^{0}$, (e) $Y = d^{1}$, (f) $Y = d^{3}$, and (g) $Y = d^{5}$. As a reference, the rays paths for the Laplace's equation is shown in (h). The relative full-mesh resolution is 4.17e-03.

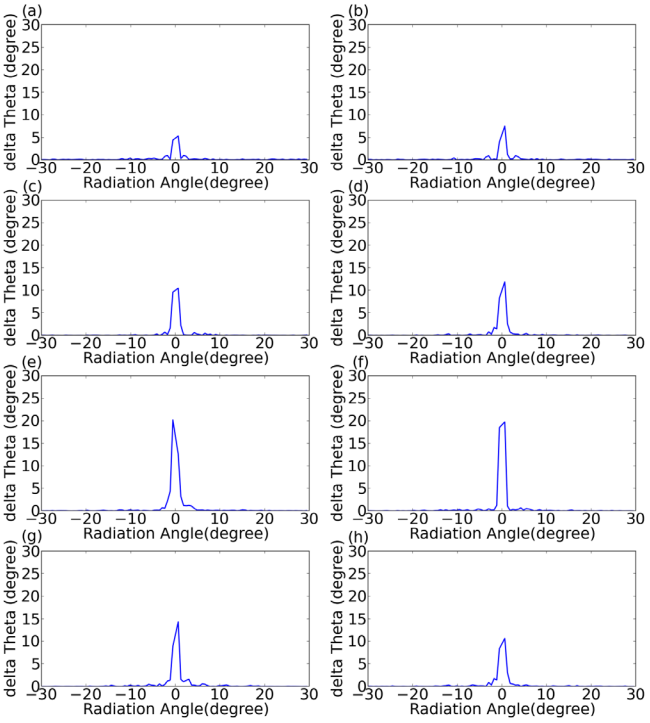

Fig. 6. The dependences of the cloaking performance on the radiation angle for the distributions of **ε** and **μ** obtained by the FEM-based solution of the Navier's equation with various distribution of Young's modulus (Y); (a) $Y = d^{-5}$, (b) $Y = d^{-3}$, (c) $Y = d^{-1}$, (d) $Y = d^{0}$, (e) $Y = d^{1}$, (f) $Y = d^{3}$, and (g) $Y = d^{5}$. As a reference, the profile for the Laplace's equation is shown in (h). The relative full-mesh resolution is 4.17e-03.

4. Discussions

4.1. Effects of Young's Modulus on the Distribution of ε and μ

Let us consider the effects of Young's modulus on the distributions of **ε** and **μ**. From Eqs. (4a)-(4c), Young's modulus is found to change the distributions of **ε** and **μ** through the value of f given by Eq. (5). The expression of f can be rewritten by

$$f = \frac{dr'}{dr} = \frac{d(r + U_r)}{dr} = 1 + \frac{dU_r}{dr}, \qquad (7)$$

where U_r is the displacement in the radial direction and dU_r/dr the strain in the radial direction. Equation (7) shows that the value of f increases with increasing the value of the strain. Since the space transformation from (r, ϕ, z) to (r', ϕ', z') compresses the region in the radial direction, the strain becomes a negative value. On the other hand, the larger value of Young's modulus is considered to give the smaller absolute value of the strain from the viewpoint of continuum mechanics. Therefore, the larger value of Young's modulus gives the larger value of the strain, leading to the larger value of f.

Based on the effects of Young's modulus on the value of f described above, the distributions of Young's modulus which increase from the inner boundary to the outer boundary, such as $Y = d^{1}$, d^{3}, and d^{5}, are considered to give smaller values of f at the inner boundary than those which decrease from the inner boundary to the outer boundary, such as $Y = d^{-1}$, d^{-3}, and d^{-5}. On the other hand, the distributions of Young's modulus which increase from the inner boundary to the outer boundary are considered to give larger values of f at the outer boundary than those which decrease from the inner boundary to the outer boundary.

Shown in Fig. 7 is the relationship between r and r' for various distributions of Young's modulus. The slopes of the curves correspond to the values of f. Figure 7 indicates that the value of f at the inner boundary increases in the order from $Y = d^{5}$ to $Y = d^{-5}$. In contrast, the value of f at the outer boundary increases in the order from $Y = d^{-5}$ to $Y = d^{5}$. These results agree with the effects of Young's modulus on the value of f.

We can see that the calculated results shown in Fig. 3 and Fig. 4 can be explained by the value of f as follows. Looking at ε_r, ε_ϕ and ε_z at the outer boundary, these values can be written as follows:

$$r' \to b,\ r \to b \Rightarrow\ \varepsilon_r \to f,\ \varepsilon_\phi \to \frac{1}{f},\ \varepsilon_z \to \frac{1}{f}. \qquad (8)$$

Therefore, ε_r at the outer boundary increases with increasing f, which means that it increases in the order from $Y = d^{-5}$ to $Y = d^{5}$. On the other hand, ε_ϕ and ε_z at the outer boundary decrease with decreasing f, which means that they increase in the order from $Y = d^{5}$ to $Y = d^{-5}$.

Next we compare the slopes of ε_r and ε_z, at the inner boundary. The slopes of them can be expressed as

$$r' \to a,\ r \to 0 \Rightarrow\ \frac{d\varepsilon_r}{dr} \to \frac{f}{a},\ \frac{d\varepsilon_z}{dr} \to \frac{1}{a \cdot f}. \qquad (9)$$

Equation (9) suggests that the slope of ε_r at the inner boundary increase with increasing f, which corresponds to the order from $Y = d^{-5}$ to $Y = d^{5}$, whereas that of ε_z at the inner boundary increases with decreasing f, which corresponds to the order from $Y = d^{5}$ to $Y = d^{-5}$.

Finally we consider the value of ε_ϕ near the inner boundary, at $d = \delta$. Here δ is a very small value. The value at $r = \delta$ can be calculated as follows:

$$\varepsilon_\phi = \frac{a}{\delta \cdot f} \qquad (10)$$

This reveals that ε_ϕ near the inner boundary increase with decreasing f. That is, it increases in the order from $Y = d^{5}$ to $Y = d^{-5}$.

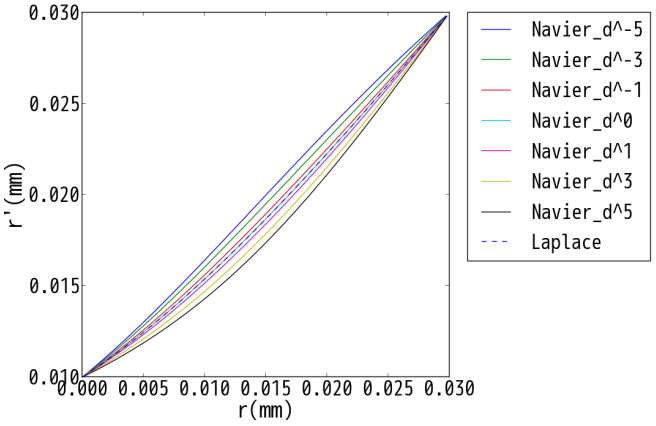

Fig. 7. The relationship between r and r' for various distributions of Young's modulus.

4.2. Effects of Young's modulus on Cloaking Performance

Shown in Fig. 8 is the cloaking performance calculated for the five relative full-mesh resolutions and the seven distributions of **ε** and **μ**. From Fig. 8, it can be seen that distributions of Y decreasing from the

inner boundary to the outer boundary, such as $Y=d^{-5}$ and $Y=d^{-3}$ tend to yield good performance. As shown in Fig. 6, the most dominant error contributing to the cloaking performance is caused by the deviation of the ray trajectories passing near the inner boundary. This deviation is due to the low accuracy of interpolation for the representation of distributions of $\boldsymbol{\varepsilon}$ and $\boldsymbol{\mu}$ inside the elements neighboring the inner boundary [31]. From Fig. 5 and Fig. 6, the deviation of the ray trajectories can be suppressed by changing from $Y=d^{5}$ *to* $Y=d^{-5}$.

The reason for this trend can be explained by the features of the distributions of $\boldsymbol{\varepsilon}$ and $\boldsymbol{\mu}$ as described in 4.1. From Fig. 3, it can be seen that with changing from $Y=d^{-5}$ to $Y=d^{5}$, ε_r and ε_z can approach zero at larger d, and ε_ϕ can approach the unlimited value at larger d. By these features, the ray passing near the inner boundary can be guided around it at the larger d as shown in Fig. 9. Therefore, the ray can escape from the region with low accuracy, leading to the successful cloaking.

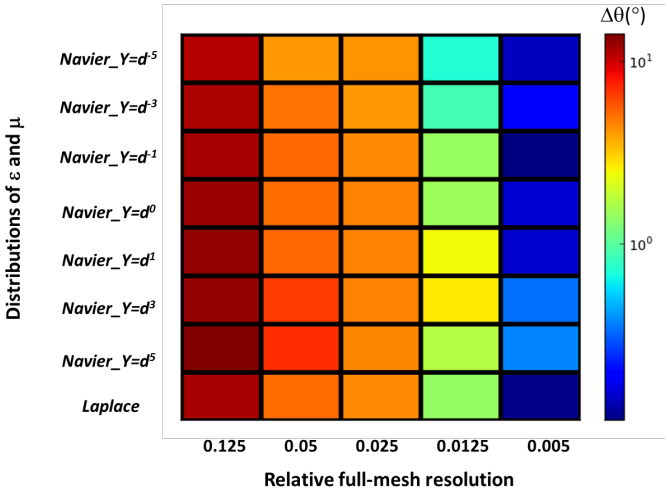

Fig. 8. The cloaking performance for the five relative full-mesh resolutions and the seven distributions of $\boldsymbol{\varepsilon}$ and $\boldsymbol{\mu}$.

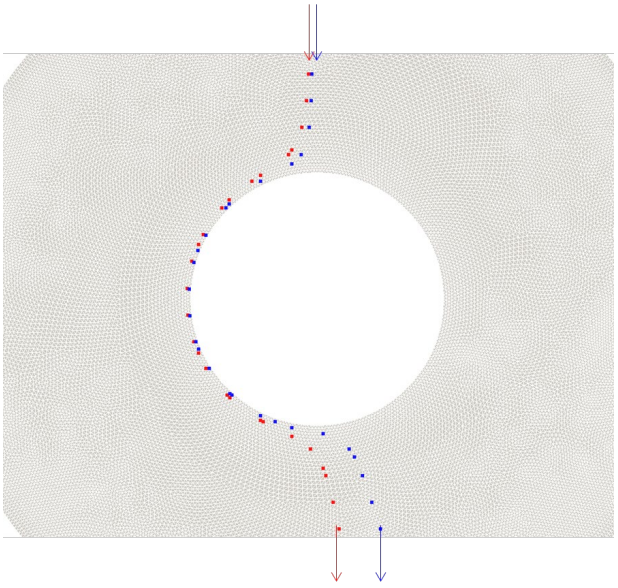

Fig. 9. The ray paths passing near the inner boundary for $Y=d^{-5}$ (the red points) and $Y=d^{5}$ (the blue points).

In order to validate that the performance of cloaking devices with other shapes can be improved by the variation of the distribution of Y, we calculate the cloaking performance of a cloaking device with a more complicated shape, which was investigated in our previous study [31]. We employ the distributions of $\boldsymbol{\varepsilon}$ and $\boldsymbol{\mu}$ obtained by the numerical method based on the FEM by employing the Navier's equation with the following three distributions of Young's modulus: (i) $Y=d^{-5}$, (ii) $Y=d^{-3}$, (iii) $Y=d^{-1}$. In addition, the distributions of $\boldsymbol{\varepsilon}$ and $\boldsymbol{\mu}$ obtained by employing the Laplace's equation are employed to be compared with the Navier's equation. The cloaking device is represented by the full-mesh representation with the relative full-mesh resolution of 1.67e-03.

The numerical result of the ray trajectories is depicted in Fig. 10. The calculated cloaking performance is shown in Table 2. It can be seen that the performance can be improved by using the distributions of Y decreasing from the inner boundary to the outer boundary in comparison with the Laplace's equation in the same way as the cylindrical cloaking device.

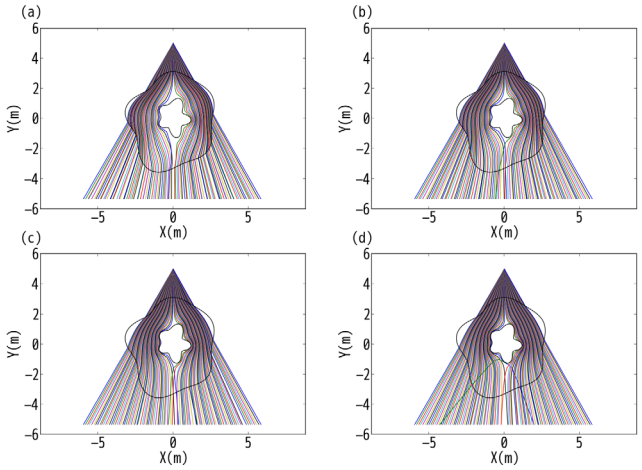

Fig. 10. The ray paths with the huge arbitrary cloaking device for the distributions of $\boldsymbol{\varepsilon}$ and $\boldsymbol{\mu}$ obtained by the FEM-based solution of the Navier's equation with various distribution of Young's modulus (Y); (a) $Y = d^{-5}$, (b) $Y = d^{-3}$, (c) $Y = d^{-1}$. As a reference, the ray paths for the Laplace's equation is shown in (d). The relative full-mesh resolution is 1.67e-03.

Table 2: Performances of the huge arbitrary cloaking device calculated for the distributions of ε and μ obtained by the FEM-based solution of the Navier's equation with various distribution of Young's modulus (*Y*) and the Laplace's equation.

Number	Relative full-mesh resolution	Equations		Δθ(°)
1	1.67e-03	Navier's Eq.	$Y=d^{-5}$	0.259
2			$Y=d^{-3}$	0.458
3			$Y=d^{-1}$	0.447
4		Laplace's Eq.		2.54

5. Conclusion

We have investigated the improvement of the cloaking performance of cylindrical cloaking by the design of the distributions of constitutive parameters. The distributions of the constituent parameters were changed by employing the Navier's equation with various distributions of Young's modulus as the partial differential equation for the numerical method calculation of the constitutive parameters based on the FEM. We have evaluated the performance by the Hamiltonian ray tracing with the full-mesh representation.

The numerical results have shown that the cloaking performance can be improved by employing the distributions of Young's modulus which decrease from the inner boundary to the outer boundary. These distributions can generate the distributions of the constituent parameters which can guide the ray around the inner boundary at the larger distance from the inner boundary. Therefore, the ray can escape from the region with low accuracy, leading to the successful cloaking. From the obtained results, we can suggest that higher values of Young's modulus near the inner boundary compared with other regions can lead to the improvement of cloaking performance as a guideline for the design of the distributions of the constituent parameters. We have confirmed that the guideline can be applied to the example of huge cloaking devices with completely arbitrary shapes.

From the viewpoint of the manufacture, the design method of distributions of the constitutive parameters can relax the condition on the resolution required for successful cloaking since the method can improve the cloaking performance at a coarse full-mesh resolution. Therefore, it is expected that the design of distributions of constitutive parameters will contribute to the realization of cloaking devices with large scale, taking into account of the finite resolution of the manufacture.

Acknowledgements

We are grateful to Mr. Toshiharu Yamamoto and Mr. Masahiro Tsukamoto with AsahiKasei Corp. for their valuable comments and discussion.

Reference

1. J. B. Pendry, D. Schurig, and D. R. Smith, "Controlling electromagnetic fields," Science **312**, 1780–1782 (2006).
2. U. Leonhardt, "Optical conformal mapping," Science **312**, 1777–1780 (2006).
3. D. Schurig, J. J. Mock, B. J. Justice, S. A. Cummer, J. B. Pendry, A. F. Starr, and D. R. Smith, "Metamaterial electromagnetic cloak at microwave frequencies," Science **314**, 977–980 (2006).
4. W. Cai, U. K. Chettiar, A. V. Kildishev, and V. M. Shalaev, "Optical cloaking with non-magnetic metamaterials," Nat. Photonics **1**, 224–227 (2007).
5. R. Beach, "Killer pillars the blinding truth," http://www.safespeed.org.uk/bike005.pdf.
6. N. Joseph, "Jaguar and Rover develops 'transparent' A-pillar and ghost car," http://www.autoblog.com/2014/12/15/jaguar-land-rover-360-virtual-urban-windscreen-transparent-pillar-follow-me-ghost-carnavigation-systems-video-official/.
7. T. Yoshida, K. Jo, K. Minamizawa, H. Nii, N. Kawakami, and S. Tachi, Transparent Cockpit: Visual Assistance System for Vehicle Using Retro-Reflective Projection Technology (IEEE, 2008), pp. 185–188.
8. M. Inami, N. Kawakami, and S. Tachi, Optical Camouflage Using Retro-Reflective Projection Technology (IEEE, 2003), pp. 348–349.
9. M. F. Schumann, S. Wiesendanger, J. C. Goldschmidt, B. Bläsi, K. Bittkau, U. W. Paetzold and M. Wegener, "Cloaked contact grids on solar cells by coordinate transformations: designs and prototypes," Optica, **2**, 850-853 (2015).
10. D. Gao, C. Qiu, L. Gao, T. Cui, and S. Zhang, "Macroscopic broadband optical escalator with force-loaded transformation optics," Opt. Express **21**, 796–803 (2013).
11. L. M. Zhong, T. M. Niu, J. Bai, and T. J. Cui, "Design of transparent cloaks with arbitrarily inner and outer boundaries," J. Appl. Phys. **107**, 124908 (2010).
12. J. Hu, X. Zhou, and G. Hu, "Nonsingular two dimensional cloak of arbitrary shape," Appl. Phys. Lett. **95**, 011107 (2009).
13. X. Wang, S. Qu, S. Xia, B. Wang, Z. Xu, H. Ma, J. Wang, C. Gu, X. Wu, L. Lu, and H. Zhou, "Numerical methods for three-dimensional electromagnetic invisible cloaks with irregular boundary shapes," in Proceedings of Progress In Electromagnetics Research Symposium, Xi'an, China (2010), pp. 1649–1652.
14. X. Wang, S. Qu, S. Xia, B. Wang, Z. Xu, H. Ma, J. Wang, C. Gu, X. Wu, L. Lu, and H. Zhou, "Numerical method of designing three-dimensional open cloaks with arbitrary boundary shapes," Photon. Nanostr. Fundam. Appl. **8**, 205–208 (2010).
15. X. Wang, S. Qu, Z. Xu, H. Ma, J. Wang, C. Gu, and X. Wu, "Three-dimensional invisible cloaks with arbitrary shapes based on partial differential equation," Appl. Math. Comput. **216**, 426–430 (2010).
16. D. Schurig, J. B. Pendry, and D. R. Smith, "Calculation of material properties and ray tracing in transformation media," Opt. Express **14**, 9794–9804 (2006).
17. M. M. Crosskey, A. T. Nixon, L. M. Schick, and G. Kovačič, "Invisibility cloaking via non-smooth transformation optics and ray tracing," Phys. Lett. A **375**, 1903–1911 (2011).
18. J. C. Halimeh and M. Wegener, "Photorealistic rendering of unidirectional free-space invisibility cloaks," Opt. Express **21**, 9457–9472 (2013).
19. J. C. Halimeh and M. Wegener, "Time-of-flight imaging of invisibility cloaks," Opt. Express **20**, 63–74 (2012).
20. J. C. Halimeh, R. Schmied, and M. Wegener, "Newtonian photorealistic ray tracing of grating cloaks and correlation-function-based cloaking-quality assessment," Opt. Express **19**, 6078–6092 (2011).
21. J. C. Halimeh and M. Wegener, "Photorealistic ray tracing of freespace invisibility cloaks made of uniaxial dielectrics," Opt. Express **20**, 28330–28340 (2012).
22. A. J. Danner, "Visualizing invisibility: metamaterials-based optical devices in natural environments," Opt. Express **18**, 3332–3337 (2010).
23. G. Dolling, M. Wegener, S. Linden, and C. Hormann, "Photorealistic images of objects in effective negative-index materials," Opt. Express **14**, 1842–1849 (2006).
24. J. C. Halimeh, R. T. Thompson, and M. Wegener, "Invisibility cloaks in relativistic motion," Phys. Rev. A **93**, 013850 (2016).
25. J. C. Halimeh and R. T. Thompson, "Fresnel-Fizeau drag: invisibility conditions for all inertial observers," arXiv:1601.04218.
26. A. Akbarzadeh and A. J. Danner, "Generalization of ray tracing in a linear inhomogeneous anisotropic medium: a coordinate-free approach," J. Opt. Soc. Am. A **27**, 2558-2562 (2010).
27. C. Qiu, A. Akbarzadeh, T. Han, and A. J. Danner, "Photorealistic rendering of a graded negative-index metamaterial magnifier," New J. Phys. **14,** 033024 (2012).
28. A. Akbarzadeh, J. A. Crosse, M. Danesh, C. Qiu, A. J. Danner, and C. M. Soukoulis, "Interplay of Optical Force and Ray-Optic Behavior between Luneburg Lenses," ACS Photonics **2**, 1384–1390 (2015).
29. T. Tanaka and O. Matoba, "Hamiltonian-based ray-tracing method with triangular-mesh representation for a large-scale cloaking device with an arbitrary shape," Applied Optics **55**, 3456-3461 (2016)
30. J. Hu, X. Zhou and G. Hu, "Design method for electromagnetic cloak with arbitrary shapes based on Laplace's equation," Opt. Express **17**, 1308-1320 (2009)
31. T. Tanaka and O. Matoba, "Evaluation and design of a large-scale cloaking device by Hamiltonian-based ray-tracing method. Part I: Full-mesh representation," submitted to J. Opt. Soc. Am. B.
32. https://www.csc.fi/web/elmer.